Supplementary Information

Taguchi Optimised Next-Generation Electric Field Assisted Patterned Poly-(vinylidene difluoride)-based Hybrid Nanogenerators and OmniGait-Sensor

Vishnu N. Sasi[1], Megha Garg[1], P Sravandas[1], Shewli Pratihar[1], Akash M. Chandran[2], Arup R. Bhattacharyya[1], Prasanna Kumar S. Mural[1]*

[1]Department of Metallurgical Engineering and Materials Science, Indian Institute of Technology Bombay, Mumbai, Maharashtra 400076, India
[2]Department of Chemical Engineering, Maulana Azad National Institute of Technology, Bhopal, Madhya Pradesh 462003, India

*Corresponding Author - Email: prasannamural@iitb.ac.in

Table of Contents

Sections	**2**
Section S1. Taguchi optimisation of NFEP	2
Section S.2 Development of patterned polymeric PVDF using NFEP	4
Section S.3 Development of different types of patterns	4
Section S.4 Effect of drying condition on the pattern and surface	5
Section S.5 Piezoelectric study of the NEPV6BTO	6
Section S.6 Thickness optimisation of PDMS layer and Piezoelectric contribution measurement	7
Section S.7 Triboelectric Energy Conversion Efficiency	8
Tables	**9**
Table S1: Minimum voltage required for initiating the continuous line drawing with respect to the tip to collector bed distance	9
Table S2: Coded L16 orthogonal array for the line width measurement of NFEP	9
Table S3: DSC crystallinity calculation	9
Table S4: PVDF β fraction calculation	10
Table S5: Comparison of the present work with similar published studies	10
Table S6: Weight of filler added to the polymer to prepare PVDF nanocomposite with different nanofiller concentrations.	11
Supporting Videos	**11**
Video S1: Near-field electrospinning process	11
Video S2: Near-field electric Patterning process	11
Video S3: LED glowing by patterned PVDF HPTNG	11
Video S4: Human kinematics and corresponding voltage response	11
References	**11**

Supplementary Information

Sections

Section S1. Taguchi optimization of NFEP

Fig. S1 Digital image illustrating the measurement of line width using a vernier calliper and the corresponding width achieved during NFEP at optimized parameters determined through Taguchi experiments.

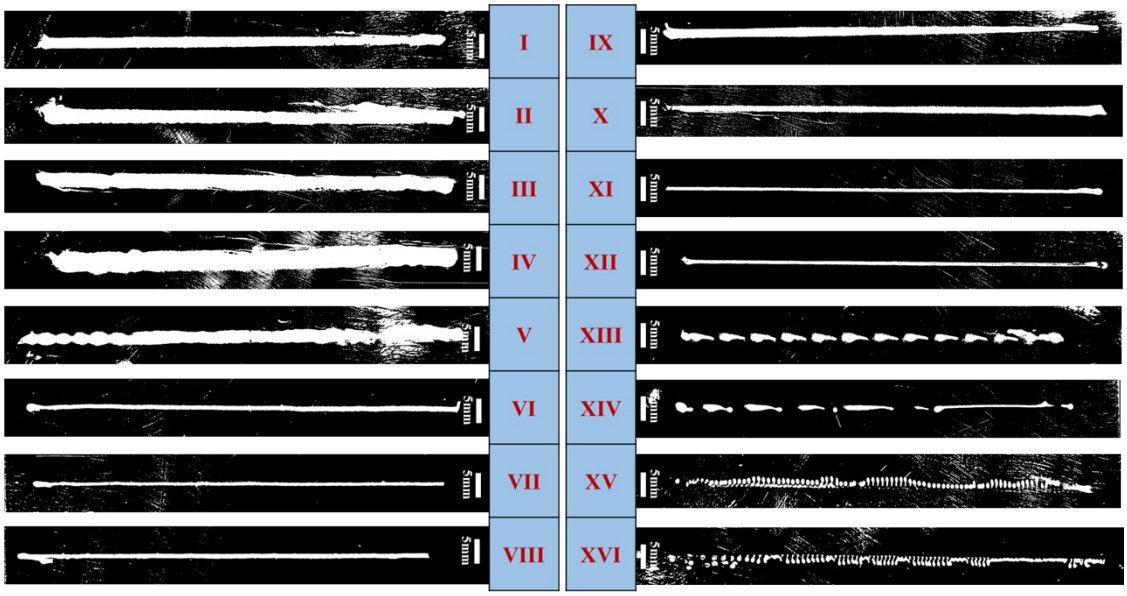

Fig. S2 Digital image of the experimental results obtained using the Taguchi L16 orthogonal array design. (All images are digitally contrast-enhanced for improved visualisation without altering structural features)

Supplementary Information

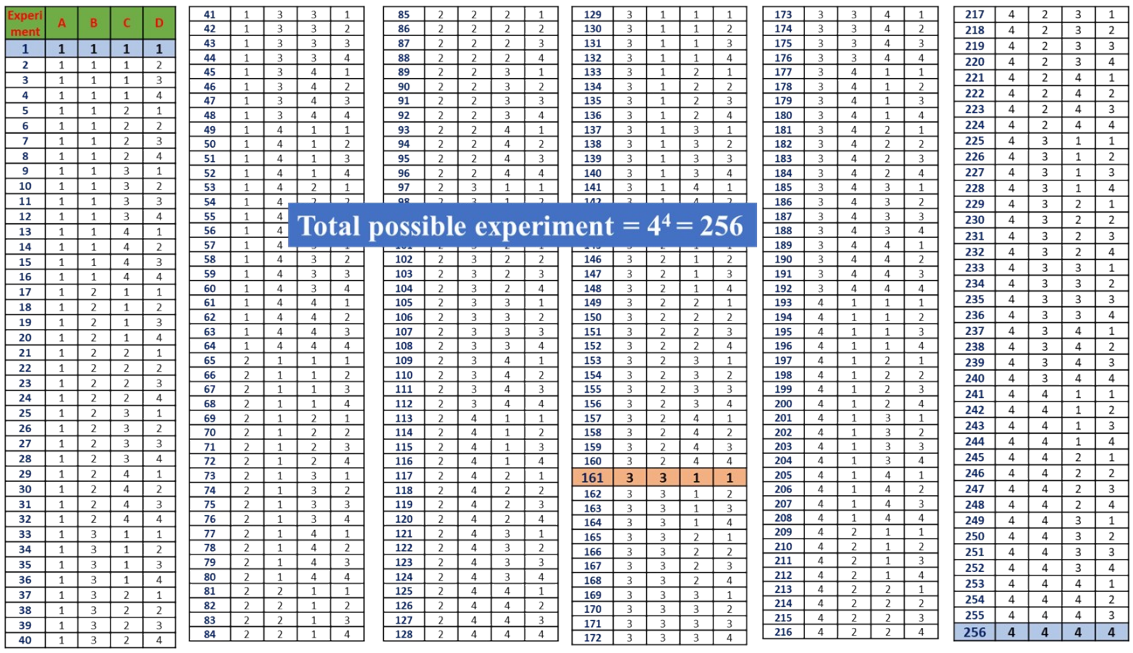

Fig. S3 Total number of experiments to perform for a four-factor four-level experimental design.

ANOVA measurement

The basis of ANOVA measurement is the splitting of the sum of squares (SS) of the level mean S/N into the sum of squares of the factor (MS Factor) and the sum of squares of error (MS $_{Error}$). This implies that the total variation in the measure results came from the variation due to the factor and the variation due to error. Average variations per degree of freedom are expressed through the mean square (MS) measurement of each factor and error. Fisher's value (F), which is the ratio of the mean square value of each factor with respect to the average variation per degree of freedom from noise (MS Error), was used to analyse each factor's effect on the output measurement.

Equations used for ANOVA calculations

- Sum of Squares

$$SS_{f=l} = \sum_{i=1}^{4} n_l(\eta_j - \bar{\eta})^2 \; where \; n_l = 4$$

- Mean Squares

$$MS_{f=l} = \frac{SS_{f=l}}{df_E}$$

- Factor degrees of freedom for a factor F (df_F)

$$df_A = 3,\ df_B = 3,\ df_C = 3,\ df_D = 3 \text{ and } \sum df_F = 12$$

- df_T = N-1 = 16-1 =15 where N = number of Orthogonal Array rows (runs)
- Error degrees of freedom

$$df_E = df_T - \sum df_F = 15\text{-}12 = 3$$

Supplementary Information

- Total sum of squares

$$SS_{Total} = \sum_{i=1}^{16} (\eta_j - \bar{\eta})^2$$

- $SS_{Error} = SS_{Total} - (SS_A + SS_B + SS_C + SS_D)$
- Fisher's statistical test - variance due to factor/variance due to error

$$F = \frac{MS_{f=l}}{MSError}$$

- Percentage Contribution of each factor

$$\%_F = \frac{SS_{f=l}}{SS_{Total}} \times 100$$

Section S.2 Development of patterned polymeric PVDF using NFEP

An appropriate computer-assisted design (CAD) of interest was developed using suitable software. The diamond mesh pattern of PVDF and its BTO nanocomposites, utilized as the active layer in this HPTNG study, was created using Inkscape software. A 2 cm × 2 cm square was drawn using the rectangle tool in Inkscape, then hatch-filled at a 45° angle with a spacing of 3 px hatch distance and cross-hatched using the KM Laser extension. Changing the hatch angle (HA) and hatch distance (HD) can create different patterns. The pattern was converted to G-code using the 4xiDraw tool, another Inkscape extension. The printing path was repeated three times by selecting the three-pass option, creating a thick enough patterned PVDF layer that could be easily removed from the bed. The G-code was communicated with the Super ES1 NFES setup through the LaserGRBL open-source software. Fig. 1c represents the schematic diagram of the near-field electric-patterning set-up.

A patterned active PVDF layer was fabricated using the optimal parameter set determined via Taguchi design of experiments. A 20 wt.% PVDF solution was prepared by adding 2 g of PVDF pellet to 8.4 mL of DMF solvent and heating and stirring at 60 °C for 4 h. The resulting thick solution was sonicated for 30 min and then transferred into a 3 mL syringe with an inner diameter of 7.8 mm and a needle diameter of 0.55 mm. The flow rate was set to 0.30 µL/s, with a collector bed-to-needle tip distance of 6 mm. After setting all experimental parameters, the NFEP process was initiated using the NFES set-up and controlled through the LaserGRBL software. A voltage of 3.5 kV was applied between the needle tip and the collector bed at the start of the NFEP process. After completing the NFEP process, the printed PVDF polymeric pattern was immediately removed from the collector bed and dried under IR light for 2 h, thereby improving its surface and porosity (Section S4).

Section S.3 Development of different types of patterns

Supplementary Information

Different patterns were created using the NFEP process. A CAD of a square mesh pattern was created by cross-hatching a 2 cm × 2 cm square at a HA of 90° and HD of 3 px (Fig. S4 Ia). A hexagonal mesh CAD pattern was obtained by hatching a 4 cm × 4 cm area at angles of 60°, 120°, and 180° at a hatch distance of 7 px (Fig. S4 IIa). Furthermore, these patterns were printed using the Taguchi-optimised parameters, and the resulting images are shown in Fig. S4 Ib and IIb. SEM image of the pattern fabricated using pure polymer of PVDF in Fig. S4 Ic and IIc, and PVDF nanocomposites are shown in Fig. S4 Id and IId.

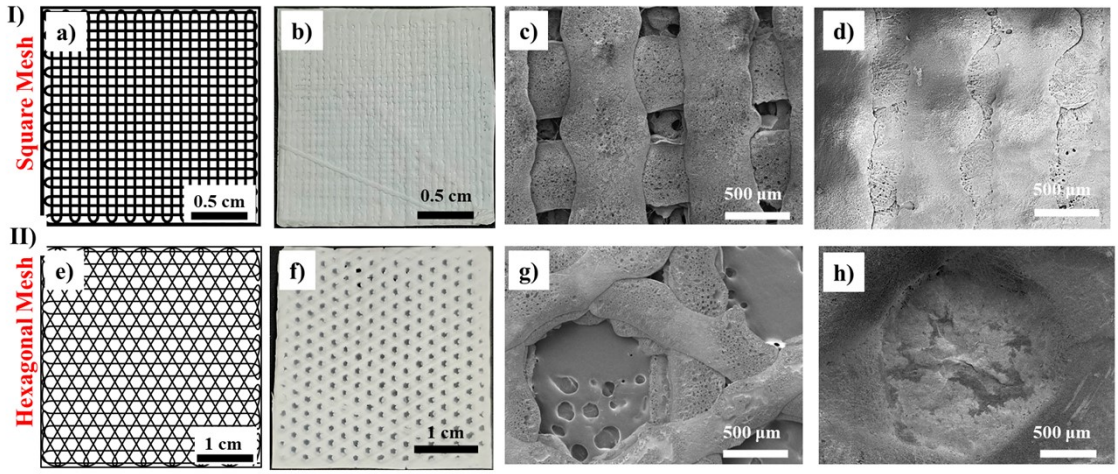

Fig. S4 Different patterns developed using NFEP. I) Square mesh pattern a) CAD design. b) Digital image of patterned PVDF. c) SEM image of pure PVDF. d) SEM image of PVDF/BTO polymer nanocomposite pattern. II) Hexagonal mesh pattern e) CAD design. f) Digital image of pure PVDF, g) SEM image of pure PVDF. h) SEM image of PVDF/BTO nanocomposite.

Section S.4 Effect of drying condition on the pattern and surface

Heat-assisted drying is one of the most widely used methods in research. In this work, the developed polymeric patterns were dried under three different conditions to assess the impact of varying drying environments on their surface morphology and integrity of the patterns. Room-temperature drying was the slowest method, taking ~16 hours to complete. IR drying drastically reduced this time to 1.5 h, while hot-air oven drying at 50 °C required only 15 min. The influence of drying temperature is evident in Fig. S5. The patterns that had dried at room temperature (Fig. S5a) appeared structurally intact at the macroscopic level; however, SEM images (Fig. S5b-d) showed partial filling of the pattern cavities due to the flow and spreading of the polymer, resulting in a smooth, non-porous surface. This is attributed to DMF's low evaporation rate at room temperature, which prolongs the drying process and thus reduces pattern fidelity. Faster solvent evaporation rates are essential for well-defined patterns with improved surface roughness. IR drying and oven drying are heat-assisted techniques that speed up the evaporation process. Patterns dried under IR light exhibited no significant change at the macroscopic level; however, SEM images (Fig. S5e) show that the faster solvent removal effectively arrested the flow of polymer, producing a surface rich in microporosity due to kinetically enhanced evaporation (Fig. S5f–h). By contrast, oven drying at 50 °C (Fig. S5i) resulted in rapid removal of DMF but significantly deteriorated the structure. The patterns thus produced became brittle and easily cracked; SEM images also show multiple fractures on their surfaces (Fig. S5j–l). Overall, IR drying provided the best balance, improving solvent

evaporation without compromising mechanical integrity while significantly enhancing surface microporosity. Therefore, all samples used in this study were dried under IR light for 1 h.

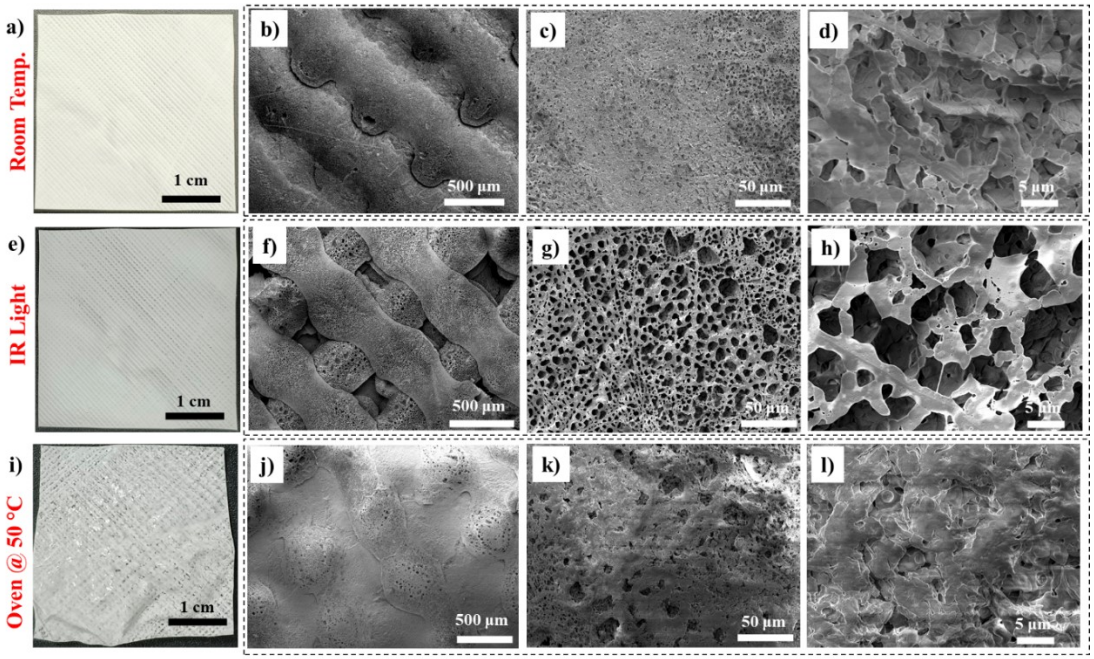

Fig. S5. Different drying conditions and the resulting pattern. Digital image of pure PVDF diamond mesh patterned polymer dried at: a) Room temperature, e) IR Light, and i) 50 °C in a hot air oven. Different magnification SEM images of the polymer dried at room temperature, under IR Light, and at 50 °C in a hot air oven: 40x (b, f, j), 500x (c, g, k), and 3000x (d, h, l), respectively.

Section S.5 Piezoelectric study of the NEPV6BTO

P–E loop measurement has been performed to evaluate the ferroelectric behaviour of the samples. The hysteresis loops confirm reversible polarisation and stable switching. Incorporation of BTO nanofillers enhances the polarisation response relative to NEPV, as evidenced by the increased loop area and higher remanent polarisation (Fig. S6a–c). This is attributed to the high dielectric constant and ferroelectric nature of BTO, which promotes stronger dipole alignment. Additionally, the breakdown voltage increases from 1300 V (NEPV) to 1600 V (NEPV6BTO), indicating improved dielectric strength and reduced leakage pathways.

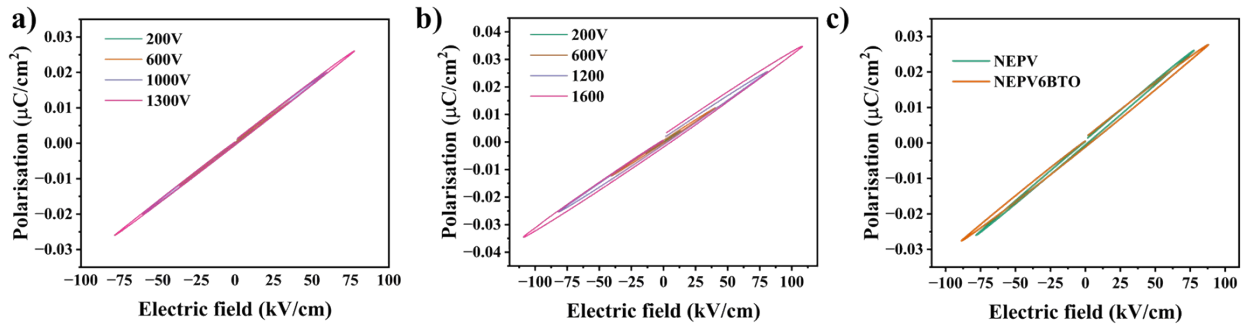

Supplementary Information

Fig. S6 Polarisation–electric field (P–E) hysteresis loops of the samples measured under an applied electric field. a) NEPV, b) NEPV6BTO, c) comparison between NEPV and NEPV6BTO at an applied voltage of 1200V

Section S.6 Thickness optimisation of PDMS layer and Piezoelectric contribution measurement

The PDMS layer thickness was optimised by fabricating counter layers with varying thicknesses. It was found that a thickness of 0.2 mm yielded the highest output of 85 V at 100 N and 20 Hz when paired with the NEPV6BTO sample. A further increase in force led to a reduction in the peak-to-peak voltage, as shown in Fig. S7a. This decrease is attributed to the polymer system's limited ability to recover strain under higher stress and frequency, particularly at greater thicknesses. At elevated frequencies, the rapid loading–unloading cycles do not allow sufficient time for the polymer to return to its original shape, resulting in reduced HPTNG output.[1], [2], [3]

Fig. S7b illustrates the schematic of the complete piezoelectric device, where the patterned polymer is sandwiched between two copper electrodes and encapsulated via thermal lamination using a PET sheet. The PET layer is selected for its relatively neutral triboelectric behaviour, thereby minimising undesired triboelectric contributions. The voltage, current, and power density outputs of the fabricated piezoelectric devices based on NEPV and NEPV6BTO were analysed and are shown in Fig. S7c and d. Fig. S7e demonstrates the complete reversibility of the signal upon reversing the external circuit connections. This confirms that the measured output originates from a true piezoelectric response, with negligible contribution from triboelectric effects.[4] The measurement results demonstrate that the maximum piezoelectric contribution under an applied force of 100 N at 20 Hz is ~7 V, with a corresponding current of ~0.4 µA.

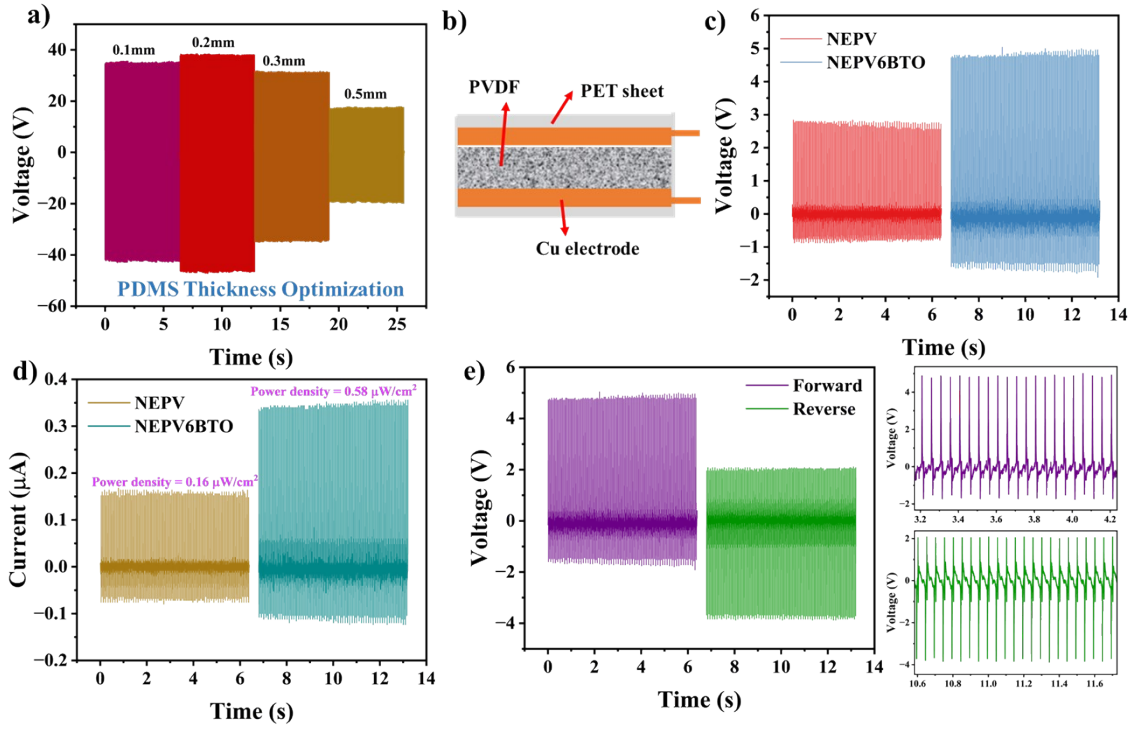

Fig. S7. (a) Thickness optimisation of the PDMS layer. (b) Schematic diagram of the fabricated piezoelectric device. Piezoelectric output of NEPV and NEPV6BTO (c) voltage

(d) current, and corresponding power output (e) demonstration of piezoelectric reversibility upon reversing the external circuit connection

Section S.7 Device Energy Conversion Efficiency

Constant Force (Impact) Loading Model:- Contact-Separation Mode Device

1. **Parameters**

Applied force (F)	100 N
Frequency (f)	20 Hz
Power density	66.8 μW cm^{-2}
Device area (A)	2 cm × 2 cm = 4 cm^2
Initial thickness (t_1)(t_{PVDF} + t_{PDMS})	0.18mm +0.20 mm = 0.38 mm
Compressed thickness (t_2)	0.27 mm

2. **Electrical Power Output**

The total electrical power output is calculated from the given power density and device area:

P_{elec} = Power Density × A = 66.8 μW/cm^2 × 4 cm^2 = 267.2 μW per cycle

$P_{elec} = 2.672 \times 10^{-4}$ W

3. **Mechanical Power Input**

3.1 Displacement per Cycle

The polymer film undergoes a thickness change from 0.38 mm to 0.27 mm under the applied force:

$\Delta x = t_1 - t_2 = 0.38 - 0.27 = 0.11$ mm $= 1.1 \times 10^{-4}$ m

3.2 Constant Force loading

Under the constant force loading, assumption, the full 100 N acts through the entire displacement.

3.3 Mechanical Work per Cycle

$W_{mech} = F \times \Delta x = 100$ N $\times 1.1 \times 10^{-4}$ m $= 1.1 \times 10^{-2}$ J/cycle

W_{mech} = 11.0 mJ/ cycle

3.4 Mechanical Power

$P_{mech} = W_{mech} \times f = 0.011$ J × 20 Hz = 0.22 W

P_{mech} = 220 mW

4. **Device Energy Conversion Efficiency**

The energy conversion efficiency is defined as the ratio of the harvested electrical power to the input mechanical power:

$\eta = P_{elec} / P_{mech} \times 100\%$

Supplementary Information

$\eta = (2.672 \times 10^{-4}\ W) / (0.22\ W) \times 100\%$

η = ~0.121%

Tables

Table S1: Minimum voltage required for initiating the continuous line drawing with respect to the tip to collector bed distance

Tip to collector bed distance (mm)	Applied Voltage (kV)
15	5.4
10	4.2
9	3.9
8	3.6
7	3.4
6	3.3

Table S2: Coded L16 orthogonal array for the line width measurement of NFEP

	Input parameters				Output Parameter			
Experiment No.	**Factor A**	**Factor B**	**Factor C**	**Factor D**	**Trial 1**	**Trial 2**	**Trial 3**	**η_i**
I	1	1	1	1	?	?	?	?
II	1	2	2	2	?	?	?	?
III	1	3	3	3	?	?	?	?
IV	1	4	4	4	?	?	?	?
V	2	1	2	3	?	?	?	?
VI	2	2	1	4	?	?	?	?
VII	2	3	4	1	?	?	?	?
VIII	2	4	3	2	?	?	?	?
IX	3	1	3	4	?	?	?	?
X	3	2	4	3	?	?	?	?
XI	3	3	1	2	?	?	?	?
XII	3	4	2	1	?	?	?	?
XIII	4	1	4	2	?	?	?	?
XIV	4	2	3	1	?	?	?	?
XV	4	3	2	4	?	?	?	?
XVI	4	4	1	3	?	?	?	?

Table S3: DSC crystallinity calculation

	ΔH_m (W/g)	**$\Delta H_{m(100)}$ (W/g)**	**Weight fraction (φ)**	**% Crystallinity (Xc)**	**Temperature (°C)**
NEPV	24.12	104.5	0	23.08	163.9
NEPV4BTO	26.7	104.5	0.04	26.61	163.7
NEPV6BTO	26.96	104.5	0.06	27.45	163.8
NEPV8BTO	24.46	104.5	0.08	25.44	163.7

NEPV10BTO	23.25	104.5	0.1	24.72	163.8

Table S4: PVDF β fraction calculation

	α transmittance (T_α)	**β transmittance (T_β)**	**α absorbance (A_α)**	**β absorbance (A_β)**	**F(β)**
Wavenumber	763 cm^{-1}	840 cm^{-1}	-log10 (T_α)	-log10 (T_β)	$=A_\beta*100/(1.26*A_\alpha+A_\beta)$
Pure PV	0.978	0.976	0.0097	0.0106	46.43
NEPV	0.894	0.753	0.0487	0.1232	66.77
NEPV4BTO	0.914	0.773	0.0391	0.1118	69.44
NEPV6BTO	0.958	0.795	0.0186	0.0996	80.93
NEPV8BTO	0.945	0.766	0.0246	0.1158	78.90
NEPV10BTO	0.910	0.682	0.0410	0.1662	76.31

Table S5: Comparison of the present work with similar published studies

Materials used for the Nanogenerator	**Device dimension (cm^2)**	**Peak to Peak voltage (V)**	**Current (μA)**	**Power density (μW cm^{-2})**	**Reference**
P(VDF-TrFE)-PDMS	10.8 ×1.2	13.1	0.046	0.0106	[5]
ZnO/PVDF- PDMS	5 × 5	6.8	0.8	0.130	[6]
MXene/PVDF- PEI	3 ×2	40	43	4.08	[7]
ZnO/PVDF-PDMS	-	7.3	-	-	[8]
PVDF/CdS - Glass	2.5 × 2.5	27	0.53	0.8	[9]
PDMS/PVDF-MoS_2		211	1.6	104.5	[10]
Al-ZnO/PVDF/PDMS/C	4.5 cm diameter	40	0.28	7	[11]
PVDF/PDMS	0.5 × 2	88	5.85	28.6	[12]
PVDF-BTO/TPU	3 × 3	73	7.7	6.18	[13]
BTO-PVDF/PDMS	5 × 1	20.51	0.86	3.01	[14]
$BaTiO_3$/PVDF-PDMS	**2 × 2**	**88.5**	**5.2**	**66.8**	**This work**

Table S6: Weight of filler added to the polymer to prepare PVDF nanocomposite with different nanofiller concentrations.

Weight %	Weight	Weight %	Weight of	Solvent	Wt.%	Weight of

Supplementary Information

of PVDF (%)	of PVDF (g)	of DMF (%)	solvent (g)	(mL)	Filler (wt.%)	filler (g)
20	2	80	8	8.4	0	0
20	2	80	8	8.4	4	0.083
20	2	80	8	8.4	6	0.128
20	2	80	8	8.4	8	0.174
20	2	80	8	8.4	10	0.222

Supporting Videos

Video S1: Near-field electrospinning process

Video S2: Near-field electric Patterning process

Video S3: LED glowing by patterned PVDF HPTNG

Video S4: Human kinematics and corresponding voltage response

References

[1] X. S. Zhang *et al.*, "Frequency-multiplication high-output triboelectric nanogenerator for sustainably powering biomedical microsystems," *Nano Lett.*, vol. 13, no. 3, pp. 1168–1172, Mar. 2013, doi: 10.1021/nl3045684.

[2] X. Shen *et al.*, "Punching pores on cellulose fiber paper as the spacer of triboelectric nanogenerator for monitoring human motion," *Energy Reports*, vol. 6, pp. 2851–2860, Nov. 2020, doi: 10.1016/j.egyr.2020.10.011.

[3] M. Navaneeth *et al.*, "A medical waste X-ray film based triboelectric nanogenerator for self-powered devices, sensors, and smart buildings," *Environmental Science: Advances*, vol. 2, no. 6, pp. 848–860, Apr. 2023, doi: 10.1039/d3va00018d.

[4] A. R. Bhat, V. N. Sasi, S. Pratihar, A. M. Chandran, and P. K. S. Mural, "Signal Generation Mechanisms with Isolated and Characterized Piezo/Tribo Signals for Precise Energy Harvesting Analysis: A Pathway to Integrated Hybrid Nanogenerator Fabrication," *ACS Appl. Energy Mater.*, vol. 8, no. 10, pp. 6528–6544, May 2025, doi: 10.1021/acsaem.5c00448.

[5] J. Wang, C. C. Chen, C. Y. Shie, T. T. Li, and Y. K. Fuh, "A hybrid sensor for motor tics recognition based on piezoelectric and triboelectric design and fabrication," *Sens. Actuators A Phys.*, vol. 342, p. 113622, 2022, doi: https://doi.org/10.1016/j.sna.2022.113622.

[6] W. Dong, M. Zhang, T. Peng, Y. Peng, Z. He, and D. Yao, "PVDF/ZnO-PDMS-based hybrid piezoelectric–triboelectric nanogenerator for self-powered sensing and

harvesting vibration energy on the train bogies," *J. Mater. Sci.*, vol. 60, no. 37, pp. 17106–17120, 2025, doi: 10.1007/s10853-025-11362-y.

[7] M. M. Hasan *et al.*, "Scalable Fabrication of MXene-PVDF Nanocomposite Triboelectric Fibers via Thermal Drawing," *Small*, vol. 19, no. 6, p. 2206107, Feb. 2023, doi: https://doi.org/10.1002/smll.202206107.

[8] K. Song and K. Y. Shin, "ZnO/PVDF Nanogenerators with Hemisphere-Patterned PDMS for Enhanced Piezoelectric Performance," *Polymers (Basel).*, vol. 17, no. 15, Aug. 2025, doi: 10.3390/polym17152041.

[9] A. Mondal, M. Faraz, and N. Khare, "Temperature-tuned enhanced performances of PVDF-based flexible triboelectric nanogenerator," *Appl. Phys. Lett.*, vol. 124, no. 10, p. 103901, Mar. 2024, doi: 10.1063/5.0189028.

[10] V. Singh and B. Singh, "PDMS/PVDF- MoS2 based flexible triboelectric nanogenerator for mechanical energy harvesting," *Polymer (Guildf).*, vol. 274, p. 125910, 2023, doi: https://doi.org/10.1016/j.polymer.2023.125910.

[11] X. Yang and W. A. Daoud, "Triboelectric and Piezoelectric Effects in a Combined Tribo-Piezoelectric Nanogenerator Based on an Interfacial ZnO Nanostructure," *Adv. Funct. Mater.*, vol. 26, no. 45, pp. 8194–8201, Dec. 2016, doi: https://doi.org/10.1002/adfm.201602529.

[12] Q. Chen *et al.*, "Hybrid Piezoelectric/Triboelectric Wearable Nanogenerator Based on Stretchable PVDF–PDMS Composite Films," *ACS Appl. Mater. Interfaces*, vol. 16, no. 5, pp. 6239–6249, Feb. 2024, doi: 10.1021/acsami.3c15760.

[13] S. Bairagi, M. Zada, C. Otesteanu, and C. Menon, "Electro-active phase assisted all-fiber triboelectric nanogenerator (AF-TENG) for energy harvesting and human joint angle monitoring," *Nano Energy*, vol. 150, p. 111784, 2026, doi: https://doi.org/10.1016/j.nanoen.2026.111784.

[14] W. Dong, M. Li, C. Chen, K. Xie, J. Hong, and L. Yang, "Flexible hybrid self-powered piezo-triboelectric nanogenerator based on BTO-PVDF/PDMS nanocomposites for human machine interaction," *Sci. Rep.*, vol. 15, no. 1, p. 15991, 2025, doi: 10.1038/s41598-025-00686-z.